JOURNAL OF GUIDANCE, CONTROL, AND DYNAMICS
Vol. 31, No. 5, September–October 2008

Skip Entry Trajectory Planning and Guidance

Christopher W. Brunner* and Ping Lu†
Iowa State University, Ames, Iowa 50011

DOI: 10.2514/1.35055

A numerical predictor–corrector method for trajectory planning and closed-loop guidance of low-L/D vehicles during the skip entry phase of a lunar-return mission is presented. The strategy calls for controlling the trajectory by modulation of the magnitude of the vehicle's bank angle. The magnitude of the bank angle used in the skip phase is determined by satisfying the downrange requirement to the landing site. The problem is formulated as a nonlinear univariate root-finding problem. Full three-degree-of-freedom nonlinear trajectory dynamics are included to achieve high accuracy of the landing prediction. In addition, the proposed approach automatically yields a direct-entry trajectory when the downrange is such that a skip entry is no longer necessary. The same algorithm repeatedly applied onboard in every guidance cycle realizes closed-loop guidance in the skip entry phase. A number of issues are identified and addressed that are critical in closed-loop implementations. Extensive three-degree-of-freedom dispersion simulations are performed to evaluate the performance of the proposed approach, and the results demonstrate very reliable and robust performance of the algorithm in highly stressful dispersed conditions.

I. Introduction

FOR entry vehicles with relatively low-lift-to-drag L/D ratios, a known strategy since the Apollo era for achieving long downrange is to allow the vehicle to skip out of the atmosphere [1–7]. Figure 1 shows an illustration of this concept with the first entry, skip, then reentry of the atmosphere, and final entry phase to the landing site. The atmospheric exit condition of the skip phase, including downrange, velocity, and flight-path angle, must be such that they lead to correct entry conditions for the final phase for successful landing. The two essential functions of the entry guidance system in the skip phase are to plan the skip trajectory and provide guidance commands to ensure the satisfaction of the required conditions at the atmospheric exit. Given the critical importance of the skip trajectory and the relatively limited maneuverability of such vehicles, early in the Apollo program, it was already realized that the skip trajectory would need to be designed onboard, based on the actual flight condition.

Because of severely limited onboard computation capability at the time, the Apollo skip entry trajectory-planning algorithm had to rely on a number of approximations and empirical equations to arrive at analytical expressions that relate the bank-angle magnitude to the exit condition of the skip trajectory [1,2]. The corresponding downrange in the skip phase is also obtained by approximate analytical equations. From a particular skip exit state, the range in the Kepler phase is computed analytically, based on Keplerian orbit theory. The downrange in the final entry phase is estimated by using the adjoints to the linearized trajectory dynamics as the sensitivity coefficients. In this way, the total downrange is determined as an approximate analytical function of the bank-angle magnitude in the skip phase. A secant iteration scheme is employed to find the required bank-angle magnitude. Once such a reference trajectory is found, the Apollo guidance system commands the bank angle to track the reference velocity and rate of altitude profiles by a linear guidance law. The various approximations and linearization assumptions have been found to limit the accuracy of the guidance, especially in the case in which the downrange is relative long [5,6]. This inaccuracy can have a significant adverse impact on the success of the mission. For instance, for the class of entry vehicles such as the Apollo and Orion Crew Exploration Vehicles (CEV), the maximum variations in the downrange for a nominal entry mission that the vehicle can accommodate in the final phase are on the order of ± 370 km (200 nm), due to the limited L/D ratio. Significant errors arising from incorrect atmospheric exit conditions in the skip phase could render the vehicle unable to satisfy the remaining range requirement in the final phase.

For low-lifting vehicles, various other methods have been suggested for atmospheric guidance. For direct entry, one method is to extend the space shuttle entry guidance approach to track a precomputed drag profile [8–11]. Analytic approaches using asymptotic expansions and optimal control techniques have been attempted for skip entry and aeroassist maneuvers [3,4,12,13]. With the advent of flight computers, onboard calculation of a trajectory has become viable through the use of numerical predictor–corrector methods [5–7,13–17]. These methods are not limited by the validity of the simplifications, approximations, and empirical assumptions necessary for any analytical treatment; thus, they hold greater potential to be more accurate and adaptive. In this paper, a numerical predictor–corrector approach motivated by similar principles is developed for the skip entry problem.

The numerical method presented in this paper is for purposes of both trajectory planning and closed-loop guidance for a low-L/D vehicle during the skip entry phase. In the trajectory planning, a linear bank-angle magnitude profile is sought in skip phase and a specified constant bank angle (e.g., 70 deg) is flown in the final phase. The trajectory from the current condition in the skip phase to the end of the final phase is numerically simulated. The initial magnitude of the linear bank-angle profile used in the skip phase is determined by satisfying the downrange requirement to the landing site. The search for the required initial bank-angle magnitude is formulated as a nonlinear univariate root-finding problem. Unlike the Apollo skip phase trajectory-planning approach, this method does not rely on approximations and empirical equations. Therefore, full 3-DOF nonlinear trajectory dynamics, including the effects of Earth rotation, can be used in the trajectory planning without any difficulty for achieving high accuracy of the landing prediction. In addition, the proposed approach automatically yields a direct-entry trajectory without a skip out of the atmosphere by the vehicle when the downrange is such that a skip entry is no longer necessary.

When the same algorithm is used in every guidance cycle update during the skip phase, the solution effectively provides a closed-loop bank-angle-magnitude command. No additional tracking guidance law is needed. The sign of the bank angle is determined by bank-reversal

Presented as Paper 6777 at the AIAA Guidance, Navigation, and Control Conference and Exhibit, Hilton Head, SC, 20–23 August 2007; received 8 October 2007; revision received 8 February 2008; accepted for publication 15 February 2008.

*Graduate Research Assistant, Department of Aerospace Engineering, 2271 Howe Hall, Room 1200. Student Member AIAA.

†Professor, Department of Aerospace Engineering, 2271 Howe Hall, Room 1200; plu@iastate.edu. Associate Fellow AIAA.

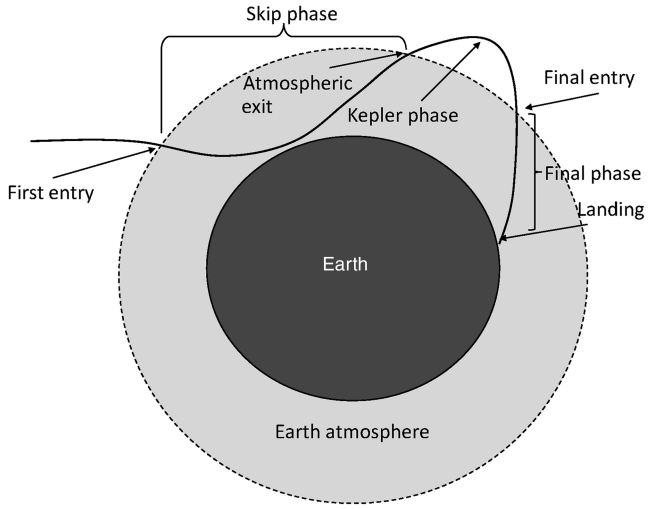

Fig. 1 Skip entry trajectory for lunar-return mission.

logic that keeps the crossrange within an envelope and steers the vehicle to the landing site. Closed-loop guidance in the final phase is provided by another robust numerical predictor–corrector method that was specifically developed for final-phase entry guidance [17].

The performance and robustness of the proposed algorithm also hinge on several critical issues. The impact of the transient effects of bank reversals in the skip phase proves to be significant on the subsequent trajectory. Thus, bank reversals should be executed in the direction of minimizing the time of reversals during the skip. It is found to be very helpful in achieving the required high precision to use first-order fading-memory filters to continuously shape the lift and drag acceleration profiles in the planning and guidance algorithm. This is particularly so in the presence of large atmospheric and aerodynamic uncertainties. For long skip trajectories, Earth rotation tends to cause a final-phase crossrange that is larger than the vehicle can recover from, mainly in the presence of large dispersions with high drag and low lift. Taking advantage of the planning algorithm, an automated targeting bias logic is developed for the skip phase to compensate for such an occurrence.

Extensive 3-DOF dispersion simulations using a capsule vehicle model similar to that of the Orion CEV are conducted for several lunar-return mission scenarios with a wide spread of initial downranges. The dispersions include those in entry condition at the first entry interface due to deorbit condition dispersions, aerodynamic coefficients, vehicle mass, and atmospheric density. The end-to-end performance of the algorithms in guiding the vehicle through skip entry to the end of the final-phase entry flight is evaluated. In the 50,000 dispersed simulations, 99.998% of the trajectories end within 2.5 km of the landing site under highly stressful dispersed conditions. The test results establish the viability and promising potential of this skip entry trajectory planning and guidance approach.

II. Problem Formulation

To simulate a spacecraft's entry flight, the dimensionless equations of three-dimensional motion for a point mass about a rotating Earth are integrated. These equations are [18]

$$\dot{r} = V\sin\gamma \tag{1}$$

$$\dot{\theta} = \frac{V\cos\gamma\sin\psi}{r\cos\phi} \tag{2}$$

$$\dot{\phi} = \frac{V\cos\gamma\cos\psi}{r} \tag{3}$$

$$\dot{V} = -D - \frac{\sin\gamma}{r^2} + \Omega^2 r\cos\phi(\sin\gamma\cos\phi - \cos\gamma\sin\phi\cos\psi) \tag{4}$$

$$V\dot{\gamma} = L\cos\sigma + \left(V^2 - \frac{1}{r}\right)\frac{\cos\gamma}{r} + 2\Omega V\cos\phi\sin\psi + \Omega^2 r\cos\phi(\cos\gamma\cos\phi + \sin\gamma\cos\psi\sin\phi) \tag{5}$$

$$V\dot{\psi} = \frac{L\sin\sigma}{\cos\gamma} + \frac{V^2\cos\gamma\sin\psi\tan\phi}{r} - 2\Omega V(\tan\gamma\cos\psi\cos\phi - \sin\phi) + \frac{\Omega^2 r\sin\psi\sin\phi\cos\phi}{\cos\gamma} \tag{6}$$

with

$$D = \frac{\rho(V_s V)^2 S_{\text{ref}} C_D}{2mg_0} \tag{7}$$

$$L = \frac{\rho(V_s V)^2 S_{\text{ref}} C_L}{2mg_0} \tag{8}$$

The differentiation is with respect to a dimensionless time:

$$\tau = \frac{t}{\sqrt{R_0/g_0}} \tag{9}$$

where r is the distance from the center of the Earth, θ is the longitude, ϕ is the latitude, V is the atmospheric-relative velocity, γ is the flight-path angle of the relative velocity, ψ is the heading angle of the relative velocity vector measured from north (positive in a clock wise direction), σ is the bank angle measured positive to the right from the view inside the vehicle, the Earth's rotation rate is $\Omega =$ 7.2921151e-5 rad/s and then nondimensionalized by the scaling factor $\sqrt{R_0/g_0}$, S_{ref} is the reference area, ρ is the local atmospheric density, D is the drag force, L is the lift force, C_D is the coefficient of drag, C_L is the coefficient of lift, m is the spacecraft mass, and g_0 is the acceleration due to gravity at the Earth's surface (0.00981 km/s^2). Note that r is scaled by the Earth's radius $R_0 = 6378.135$ km, and V is scaled by the dimensionless velocity:

$$V_s = \sqrt{R_0 g_0} \tag{10}$$

In the planning of the trajectory, the 1976 U.S. Standard Atmosphere is used as the atmospheric model. The equations of motion are integrated with a fourth-order Runge–Kutta method.

Initial entry conditions are assumed to be those on a lunar-return trajectory. The entry altitude is 121.9 km (400,000 ft). The velocity, flight-path angle, heading, latitude, and longitude are assumed to have been targeted via earlier deorbit maneuvers to bring the spacecraft to a point and heading that permit the guidance to ensure a safe entry. Specific cases are described further in Sec. V.C. A prespecified final velocity terminates the simulation, which is targeted toward a landing site. For the purposes of the simulation, when the vehicle has reached 150 m/s (500 ft/s) relative velocity, parachute deployment will occur and the simulation for entry flight terminates.

To control the trajectory, the bank angle is varied to achieve prespecified terminal constraints. The bank angle is tied into the flight-path angle via Eq. (5) and into the heading angle via Eq. (6). It is responsible for achieving the longitudinal and lateral constraints. The bank angle is determined by the guidance algorithm, which is described in the following section.

III. Algorithm Description

A. Trajectory Planning

In the planning of the complete entry trajectory from skip to the end of the final phase, the magnitude of the bank angle in the skip phase is parameterized as a function of the range-to-go $s_{\text{to-go}}$ until a specified threshold s_{thres}, which is set equal to 2000 km. Below s_{thres}, a fixed constant bank-angle magnitude of $\sigma_f = 70$ deg is used.

Figure 2 shows this bank-angle profile, which is continuous. Therefore, the bank-angle magnitude $|\sigma|$ at any range-to-go $s_{\text{to-go}} \geq s_{\text{thres}}$ is

$$|\sigma| = \sigma_f + (\sigma_0 - \sigma_f)\frac{s_{\text{to-go}} - s_{\text{thres}}}{s^0_{\text{to-go}} - s_{\text{thres}}}, \qquad s^0_{\text{to-go}} \geq s_{\text{to-go}} \geq s_{\text{thres}} \tag{11}$$

where $s^0_{\text{to-go}}$ is the current range-to-go. For a given bank-angle magnitude, the sign is assigned by a bank-reversal logic (more later). The corresponding skip trajectory is simulated onboard from the current condition to the end of the entry trajectory, defined by a specified velocity. Therefore, the skip-trajectory-planning problem is to determine the initial bank angle σ_0 in the bank-angle parameterization equation (11) that will meet the final condition on the miss distance to the landing site at the specified final velocity.

The choice of s_{thres} in the bank-angle parameterization is such that it represents typical downrange at the initiation of the final phase guidance. This value does not vary widely for low-L/D vehicles. Thus, the skip and Kepler phases take place from $s^0_{\text{to-go}}$ to s_{thres}. Even though bank angle has no influence on the trajectory in the Kepler phase, one reason for the parameterization in Fig. 2 is to maintain continuity of the bank angle. This feature is important in ensuring the convergence of the planning algorithm when the initial downrange is short and the trajectory does not have full skip and Kepler phases. Another benefit of the linear profile in Fig. 2 is that the skip trajectory will deplete the excess energy early in skip phase (because the bank angle has a larger magnitude). This tends to help alleviate the undesirable need to fly a very large bank angle toward the end of the skip phase and to increase the robustness of the guidance in the presence of severe atmospheric and aerodynamic uncertainties.

In the planning, the covered downrange is added as a seventh dimensionless equation of motion to integrate with the other variables, as given before:

$$\dot{s} = \frac{V\cos\gamma}{r} \tag{12}$$

The planning algorithm attempts to find the required bank angle σ_0 so that the downrange flown along the complete entry trajectory is equal to the actual range-to-go to the landing site. Through the integration of the equations of motion (1–6) and (12) with $|\sigma|$ given by Eq. (11), the search for σ_0 becomes a root-finding problem: at the current spacecraft state, find the σ_0 that will permit satisfying the downrange requirement:

$$s_{\text{miss}} = s^0_{\text{to-go}} - s_f(\sigma_0) = f(\sigma_0) = 0 \tag{13}$$

The current range-to-go $s^0_{\text{to-go}}$ is found by computing the great-circle distance from the current vehicle position to the landing site. Through integration of the equations of motion, the range flown s_f is found at the specified final velocity. The resulting distance will be positive if the spacecraft undershoots the final position and will be negative if there is an overshoot.

A secant method is used to iteratively solve Eq. (13). The iterates are generated by the equation

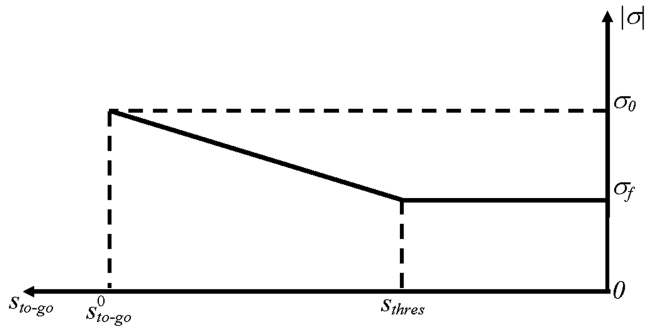

Fig. 2 Bank-angle parameterization with respect to range-to-go $s_{\text{to-go}}$.

$$x_{n+1} = x_n - \frac{x_n - x_{n-1}}{f(x_n) - f(x_{n-1})} f(x_n) \tag{14}$$

where $x = \cos\sigma_0$. To start the secant iteration scheme appropriately for the first time, an initial guess of the bank angle is required that will enable the spacecraft to reach the final velocity following a skip trajectory. An arbitrary choice could result in the vehicle bouncing off or diving steeply into the atmosphere. To find this initial bank angle, the algorithm begins by assuming an initial bank angle of 0 deg in the numerical simulation of the trajectory. If the vehicle's altitude exceeds 300 km, the spacecraft is assumed to have bounced out of the atmosphere. Then the bank-angle magnitude is incremented by a fixed amount of 2.5 deg, and the process repeats until the corresponding trajectory reenters the atmosphere following the skip and ends in the final phase with an undershoot in the final range-to-go to the landing site.

The secant iteration stops when the miss distance to the parachute deployment condition is achieved; that is, at a specified final velocity of 150 m/s (500 ft/s), the miss is less than 25 km.

To actually fly toward the end conditions, the sign of the bank angle is determined by a lateral logic that is similar to the one used in the Apollo entry guidance [1,2]. A crossrange threshold is defined as a linear function of the dimensionless velocity

$$\chi_c = c_1 V + c_0 \tag{15}$$

where c_0 and c_1 are constants set equal to 8.71e-5 and 5.21e-3 rad, respectively, for this work. Whenever the crossrange along the trajectory exceeds χ_c, as already defined, the sign of the bank angle is reversed. In the trajectory planning, the change of the bank-angle sign is achieved instantaneously, without any rate or acceleration limits. If the rate and acceleration limits are enforced, the number of bank reversals could be different in two successive iterations of the secant search. This difference will result in a discontinuity in the miss-distance function f, which will in turn cause convergence difficulties in the secant method. Instantaneous bank reversal is done to avoid this possible problem. However, it should be stressed that the bank-angle rate and acceleration limits are enforced in the guidance-command generation.

B. Closed-Loop Guidance

Once the process in the preceding section converges, a feasible skip trajectory has been found. Subsequent guidance commands can be found, in principle, by tracking this reference trajectory as done in the Apollo design. For a vehicle with low L/D value, however, achieving the kind of high precision required at the atmospheric exit (particularly in the flight-path angle) by tracking a fixed reference trajectory is difficult. This is because there are multiple competing conditions in velocity, flight-path angle, and range that need to be met, and the vehicle's limited maneuverability is inadequate to null all trajectory dispersions if they are not small.

The guidance approach adopted in this work is to use the same algorithm described in Sec. III.A repeatedly to generate a new skip trajectory using the current state as the initial condition in every guidance cycle. The magnitude of the commanded bank angle in the current cycle is then the one found in the solution. Because this solution, and thus the bank angle, depends on the current state of the trajectory, such a guidance command is closed-loop in nature. The advantages of this approach over reference tracking should be threefold:

1) The vehicle should always fly on a feasible trajectory that satisfies the required condition on range-to-go to the landing site, provided that the algorithm converges.

2) There should be no need for separate tracking guidance law and the generation and tuning of the associated gains.

3) It might be possible to further incorporate the information from the vehicle health monitoring system in the guidance solution in the event of degradation of vehicle capability due to partial system failure.

The risk, of course, is that the convergence is not achieved in one or several guidance cycles. This risk arises most likely only in the

case of severely abnormal situations. If nonconvergence occurs in just one guidance cycle, the previously obtained solution can always still be used. One of the objectives of evaluation is to assess the robustness and reliability of the algorithm through extensive testing.

On closed-loop guidance calls to the algorithm, the previously calculated bank angle is used as an initial guess for the constant to-be-flown bank angle for the skip phase, rather than beginning with a zero bank angle. If this angle is still sufficient to bring the downrange error within 25 km, the secant method is skipped and the previous bank angle is flown. Otherwise, the secant method proceeds as already noted and determines a new bank-angle magnitude.

During the finite time in a bank reversal in the actual flight, the preceding algorithm continues to run with the current state as the initial condition. The transient effects of the bank reversal will cause the algorithm to yield a somewhat different bank angle once the reversal is completed. Further discussion concerning this effect appears in Sec. IV.B. No closed-loop guidance is performed in the Kepler phase, in which aerodynamic control is ineffective.

In the final entry phase, closed-loop guidance is provided by another numerical predictor–corrector algorithm [17]. This algorithm searches for a one-parameter linear bank-angle profile that will result in the downrange flown by the vehicle being equal to the actual range-to-go to the landing site. The reader is referred to [17] for a detailed description of the algorithm and performance evaluation based on Monte Carlo simulations of the final-phase entry flight.

IV. Critical Issues in Closed-Loop Guidance

In this section, several issues critical to the success and performance of the proposed algorithm when applied in closed-loop skip entry guidance are addressed.

A. Seamless Phase Transitions

The Apollo entry guidance [1] and a recent work [19] on the Orion CEV have identified the need for improved phase transition logic in the skip entry guidance. In the Apollo entry guidance, a different strategy of guidance is used in each phase of the skip entry. Therefore, it is necessary to ensure that the transition from one phase to another will not cause difficulty in the next phase. In particular, the Apollo final-phase guidance is based on tracking of a prestored reference trajectory. If the transition into final-phase guidance does not takes place at an appropriate point, the guidance command could be severely saturated while attempting to reach the reference conditions. Another critical situation, in which smooth transition between different phases of guidance is needed, occurs when a skip trajectory is not required, as in the case in which the initial downrange is relatively short.

Because this current skip guidance algorithm generates a reference trajectory at every time step in the same manner and the guidance strategy is the same in each phase of the skip trajectory, a well-defined transition point is not necessary between two phases. The final-phase guidance is of a very similar nature in generating the bank-angle command and it integrates with the skip guidance smoothly. The starting point for the final-phase guidance is not constrained to a small neighborhood about a fixed reference trajectory, because a feasible trajectory is generated onboard based on the actual state conditions. All the traits in this approach afford seamless and easy transition between phases of the guidance logic.

Figure 3 shows the different phases in the skip entry guidance logic. The initial phase of entry is an open-loop phase, flown with a 0-deg bank angle until the aerodynamic load reaches 0.05 g_0. Following this, the skip phase is flown with a bank angle computed as described in Sec. III.A. In the normal skip entry case, the skip phase continues when the flight-path angle becomes positive. The skip trajectory is considered to have entered the Kepler phase when the load is below 0.05 g_0. The final phase begins once the range-to-go has decreased below 2000 km.

In the case in which the entry condition renders a skip trajectory completely unnecessary, this algorithm will automatically adjust to the need or lack thereof for a skip. In the skip phase, if the vehicle never has a positive flight-path angle and the range-to-go continues to decrease below 2000 km, the final-phase-guidance algorithm will take over. In such a case, a direct entry naturally takes place instead; the path of direct entry in Fig. 3 is for this scenario. This type of entry will also occur if the range-to-go is below 2000 km in the initial entry phase.

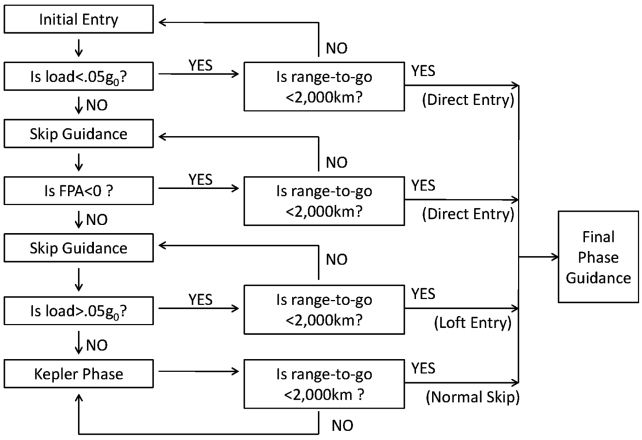

Fig. 3 Guidance phase transition logic (FPA denotes the flight-path angle).

There are also cases in which the skip is sufficiently short so that the vehicle does not leave the atmosphere (loft trajectory); thus, a Kepler phase does not exist. In this case, the skip guidance continues to run with a positive flight-path angle. Once the range-to-go is found to be less than 2000 km, the final-phase guidance is initiated, as indicated by the path of the loft trajectory in Fig. 3.

Figure 4 shows the typical altitude-versus-downrange profiles of the normal skip, loft, and direct-entry trajectories. Figure 5 plots the corresponding closed-loop bank-angle histories for these trajectories. These and future plots show the downrange-to-go in kilometers, which was converted from Eq. (13) (in radians) by multiplying by the Earth's radius R_0. The present algorithm automatically adapts to all these different situations without a priori indication of which kind of trajectory a particular mission will take.

B. Direction of Bank Reversals

The problem of steering or crossrange reduction is determined by whether to assign a positive or negative value to the computed bank-angle magnitude. The initial call to the bank-reversal logic assigns the bank angle a sign that is opposite to that of a crossrange variable χ, defined by

$$\chi = \sin^{-1}[\sin s_{\text{to-go}} \sin(\psi - \Psi)] \tag{16}$$

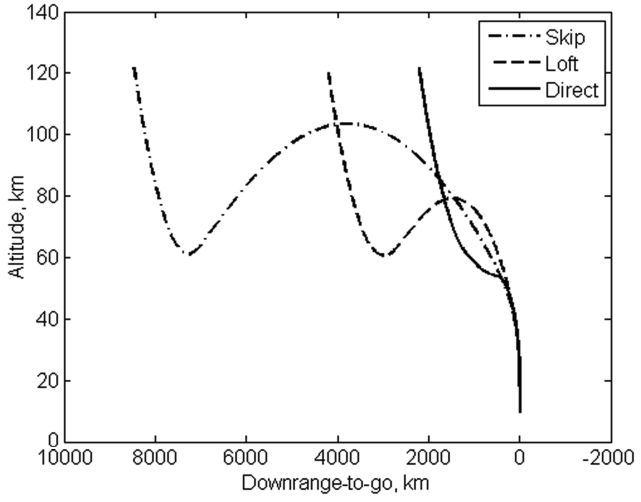

Fig. 4 Possible entry trajectory types.

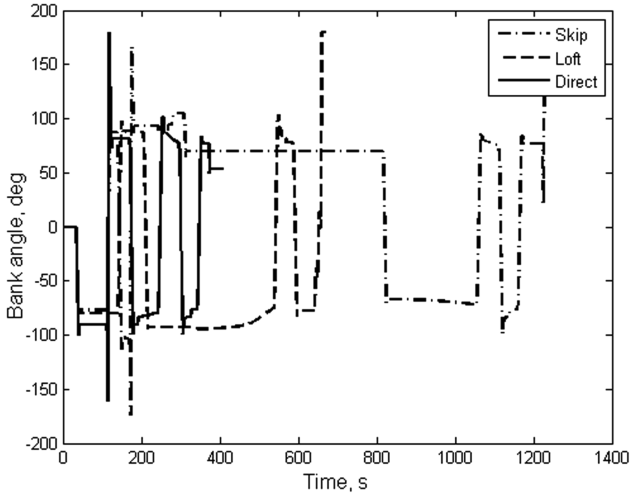

Fig. 5 Bank-angle histories for different trajectory types.

where $s_{\text{to-go}}$ is the range-to-go, ψ is the current heading angle, and Ψ is the line-of-sight azimuth angle along a great circle to the landing site. All the variables have units of radians. On future calls, the sign of the bank angle will be reversed whenever the crossrange exceeds the velocity-dependant threshold defined in Eq. (15).

In the actual flight, instantaneous bank-angle reversals are not possible as they were assumed during the planning. The bank-angle changes can occur at a metered rate that does not exceed the vehicle-dependent rate and acceleration limits. Through testing, it is found that the sensitivity of the trajectory with respect to the transient effects of the bank reversals in the skip phase is rather high, and the transition in bank reversals must be performed in an appropriate direction. If the prereversal bank angle has a magnitude greater than 90 deg, the vehicle has excess energy and a bank reversal from below (through full lift down) will help deplete some of the excess energy and cause a net effect of leaving the vehicle in the middle of the downrange envelope. However, a bank reversal from above (through full lift up) in this case will slow down the needed energy depletion. If such a wrong cycle repeats a few times, the current downrange will soon be too short for the vehicle, even if the vehicle flies with full lift down in the skip phase. The situation is similar in nature (in the opposite sense) when the prereversal bank-angle magnitude is less than 90 deg. Thus, it appears critical for the guidance system to always command the roll in a skip phase bank reversal via the short way, rather than always from above or from below. If the bank angle has a magnitude equal to 90 deg, the vehicle is on the path of zero lift to the target and has the maximum margin with respect to the downrange targeting capability.

C. Automated Targeting Bias

In the recent work by Rea and Putnam [19] on the Orion CEV and in this work, it was found necessary to target a biased landing site for longer northbound and eastbound skip trajectories in the bank-reversal logic during the skip flight. In these situations, the effects of Earth's rotation tend to cause the vehicle to have a crossrange at the start of the final phase that is larger than the final-phase guidance can compensate for, mainly in the presence of large dispersions with high drag and low lift. The target biasing is introduced to force the trajectory to veer more toward the desired direction during the skip, resulting in acceptable crossrange for the final phase. The biased landing site is only targeted during the skip phase in the lateral logic (and the longitudinal logic still uses the true landing site).

Perhaps the most effective biasing effect is achieved by moving the targeted site from the true landing site along the direction of the crossrange. The objectives to be achieved are to establish how much bias should be used, and for a specified bias, to determine what the coordinates of the biased site should be. In this work, the trajectory-planning capability of the algorithm is used to automate this process.

During the first call to the trajectory planning in the skip guidance phase, the true landing site coordinates are used. The value of the crossrange is examined at the point in the planned trajectory at which the final phase begins. If the crossrange is outside the velocity-dependent envelope in the lateral logic for bank reversal [cf. Eq. (15)], the bias logic is executed. This logic determines the bias necessary to cause the crossrange to have a sign opposite to that of the crossrange without bias. Otherwise the biasing logic is bypassed.

When the biasing is determined to be needed, the targeted site is moved away from the true landing site by a small amount $\delta\chi$ in the crossrange direction. Taking the differentials of Eq. (16) while keeping the range-to-go $s_{\text{to-go}}$ unchanged and the current vehicle heading angle ψ fixed gives

$$\delta\chi\cos\chi = \sin(s_{\text{to-go}})\cos(\psi - \Psi)(-\delta\Psi) \tag{17}$$

The small increment $\delta\chi$ is selected for the target biasing (e.g., $|\delta\chi| = 0.15$ deg to begin with). The sign of $\delta\chi$ is opposite to that of the crossrange at the beginning of the final phase without target biasing. The preceding equation determines $\delta\Psi$ because everything else in the equation is now known. The great-circle distance between the current vehicle position (θ, ϕ) and the biased site (Θ, Φ) is

$$\cos(s_{\text{to-go}}) = \sin\phi\sin\Phi + \cos\Phi\cos\phi\cos(\Theta - \theta) \tag{18}$$

The azimuth angle from the vehicle location to this biased landing site is given by

$$\sin\Psi = \frac{\sin(\Theta - \theta)\cos\Phi}{\sin(s_{\text{to-go}})} \tag{19}$$

Take differentials of Eqs. (18) and (19), keeping in mind that θ, ϕ, and $s_{\text{to-go}}$ are not changed by the biasing. The following system of linear equations is obtained as a result:

$$\begin{bmatrix} \frac{\cos(\Theta^* - \theta)\cos\Phi^*}{\sin(s_{\text{to-go}})} & -\frac{\sin(\Theta^* - \theta)\sin\Phi^*}{\sin(s_{\text{to-go}})} \\ -\cos\Phi^*\cos\phi\sin(\Theta^* - \theta) & \sin\phi\cos\Phi^* - \sin\Phi^*\cos\phi\cos(\Theta^* - \theta) \end{bmatrix} \begin{bmatrix} \delta\Theta \\ \delta\Phi \end{bmatrix} = \begin{bmatrix} \delta\Psi\cos\Psi \\ 0 \end{bmatrix} \tag{20}$$

where (Θ^*, Φ^*) are the coordinates of the true landing site. With $\delta\Psi$ already found from Eq. (17), $\delta\Theta$ and $\delta\Phi$ are found easily from system (20). The coordinates of the biased landing site are then computed by

$$\Theta = \Theta^* + \delta\Theta \qquad \Phi = \Phi^* + \delta\Phi \tag{21}$$

Note that because Eqs. (17) and (20) are linear in $\delta\chi$, $\delta\Psi$, $\delta\Theta$, and $\delta\Phi$, any change in $\delta\chi$ means the changes of the same proportion in $\delta\Theta$ and $\delta\Phi$. A new skip trajectory is planned using the biased target coordinates in Eq. (21). If the predicted crossrange condition at the beginning of the final phase still does not satisfy the preceding stated criterion for stopping the biasing, the bias $\delta\chi$ is doubled. This will lead to the increments of the same proportion in $\delta\Theta$ and $\delta\Phi$ [but system (20) does not need to be resolved again]. The biasing process is repeated using the updated biased target until the stopping criterion is met.

Table 1 Dispersions in the entry interface state and other parameters

State/parameter	Distribution	3-σ value/range (northern entry)	3-σ value/range (eastern entry)
Longitude, deg	Zero-mean Gaussian	0.0749	0.2591
Latitude, deg	Zero-mean Gaussian	0.3202	0.1790
Relative velocity, m/s	Zero-mean Gaussian	12.9053	13.3611
Flight-path angle, deg	Zero-mean Gaussian	0.1484	0.1505
Heading angle, deg	Zero-mean Gaussian	0.0973	0.0526
C_L	Zero-mean Gaussian	0.0778 (20%)	0.0778 (20%)
C_D	Zero-mean Gaussian	0.2696 (20%)	0.2696 (20%)
Mass, kg	Uniform	$\pm$5%	$\pm$5%
Atmospheric density	GRAM07 dispersed atmosphere		

Our experience shows that the typical targeting bias for the long northbound entry is about 1.5 deg and the eastbound entry about 1.0 deg.

D. Lift and Drag Filters

It is suggested in the literature and found to be true again in this work that appropriate use of estimated information on the aerodynamic and density biases is very helpful in achieving required high precision [5,14–16]. This is particularly so in the presence of large atmospheric and aerodynamic uncertainties. The dispersions include those in entry condition at the first entry interface due to deorbit condition dispersions, aerodynamics, vehicle mass, and atmospheric density. All the dispersions, except for those in the entry condition, affect only the lift and drag accelerations. During the flight, the actual values of lift and drag accelerations can be obtained from navigation data and accelerometer outputs. The effect of one source of dispersion (e.g., density) cannot be distinguished from another (e.g., aerodynamic coefficients) without another measurement (e.g., an air data system). Yet, it is realized that only the combined effect of these dispersions needs to be estimated. Toward this end, a first-order fading-memory filter is used [20]:

$$X_{n+1} = X_n + (1-\beta)(X^* - X_n) \tag{22}$$

where X^* is the current ratio of the measured variable (lift or drag acceleration) to its nominal value based on the nominal model via Eq. (7) or Eq. (8), X_n is the past filtered ratio, and $0 < \beta < 1$ is a gain (typically, a value slightly less than one) chosen to emphasize past values over the most recent value. To initialize the filter, the first past filtered ratio X_0 is set equal to one. In each skip trajectory guidance cycle, the output of this filter is used to multiply the nominal lift L (or drag D) profile in the integration/planning of the trajectory, and so the corresponding trajectory is computed based on the modified L and D.

This type of filter would be able to capture the combined effect of constant biases in mass, density, and constant percentage of dispersions in aerodynamic coefficients. However, in the testing of the algorithm, significant nonzero altitude-dependent components in the atmospheric-density dispersions are intentionally introduced via the 2007 Global Reference Atmosphere Model (GRAM07), and so the algorithm would not benefit unrealistically from this feature of the filter (see Sec. V.B). In the literature, the usefulness of such type of measures has been long recognized in atmospheric entry and aeroassist maneuvers [5,14–16]. With the exception of [16], a similar estimation has been applied to just drag or to the L/D ratio. Experience in skip entry guidance shows that application of such estimation to shape both drag and lift acceleration profiles in the online trajectory planning and guidance has clear advantages over application only to D.

A second-order filter was tested, but there was no visible improvement in results over the first-order filter.

V. Evaluation of Algorithm

A. Nominal Vehicle Model

The vehicle model used in the simulations in this paper is similar to that of the Orion Crew Exploration Vehicle. The vehicle has a capsule configuration with a base diameter of 5 m and weighs 8382 kg (18,464 lb). The vehicle flies a Mach-dependent trim angle-of-attack profile, which is about 160.2 deg in the skip phase. The L/D value is 0.289 at this trim angle of attack. The maximum rate and acceleration imposed on the bank angle in the 3-DOF simulations are $20\,\mathrm{deg/s}$ and $10\,\mathrm{deg/s^2}$, respectively, similar to those used in the literature [15]. The mission conditions correspond to those from a lunar-return mission and landing at Edwards Air Force Base (EAFB).

B. Dispersion Models

The purpose of dispersion simulations is to evaluate the performance of the guidance algorithm in the presence of significant deviations in trajectory state, vehicle, and environment modeling uncertainties. The initial entry conditions, except for altitude, are perturbed via a covariance matrix. This matrix is found by propagating the nominal entry interface conditions backward 3 h in time to when the last deorbit burn is expected to be performed. At this point, the position and velocity in inertial coordinates are each perturbed in turn by a small value and the states are propagated forward until the altitude reaches the entry interface at 121.92 km (400,000 ft) to produce the sensitivity (covariance) matrix. The deorbit-condition dispersions in position and inertial velocity components are modeled by zero-mean Gaussian dispersions. Each position component has a 3-σ value of 135 m, and each inertial velocity component has a 3-σ value of 1.35 m/s. The entry-condition dispersions are then obtained by multiplying the deorbit dispersions with the covariance matrix. The resultant dispersions in entry conditions are summarized in Table 1 for both northbound and eastbound entry missions. These entry-condition dispersions are comparable with those reported in the recent literature [21].

The vehicle mass was perturbed uniformly up to 5%. With the nominal mass of 8382 kg, this gives a range of values of 7962.9 to 8801.1 kg. For the lift and drag coefficients, existing work uses a 10%

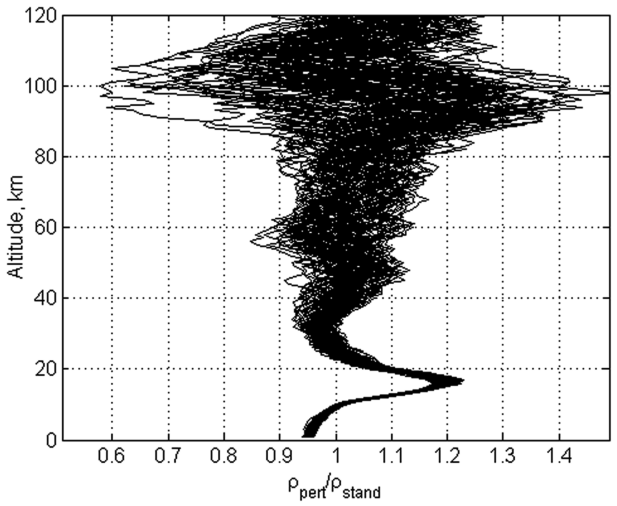

Fig. 6 Ratio of GRAM07 perturbed atmosphere to U.S. 1976 Standard Atmosphere as a function of altitude for 100 cases.

Table 2 Initial conditions

State	Northbound direct	Northbound short range	Northbound medium range	Northbound long range	Eastbound medium range
Altitude h, km	121.92	121.92	121.92	121.92	121.92
Longitude θ, deg	242.00	244.00	244.83	242.00	176.99
Latitude ϕ, deg	15.00	−3.00	−41.13	−55.00	7.14
Relative velocity V, km/s	10.98	10.98	10.98	10.98	10.60
Flight-path angle γ, deg	−5.576	−5.576	−5.576	−5.576	−5.988
Heading angle ψ, deg	0.47	0.47	0.47	0.47	54.63
Downrange s, km	2200	4200	8400	10,000	7300
Crossrange χ, km	7	204	298	42	−17

zero-mean normally distributed uncertainty in C_L or C_D [15]. To fully stress the algorithm developed in this paper, a 20% zero-mean normally distributed uncertainty from the C_L or C_D at high Mach numbers was used. This value is added to the nominally calculated C_L or C_D, giving a constant bias at all Mach numbers. The effects of constant biases in the aerodynamic coefficients are actually more demanding than with Mach-dependent uncertainty, because their influence on L/D is persistently in one direction and there is no benefit of averaging effects. At high Mach, the nominal C_L is 0.3892 and the nominal C_D is 1.3479, giving a nominal L/D of 0.289.

For the atmospheric-density dispersions, GRAM07 is used without any adjustments for wind. GRAM07 is the most recent updated version of GRAM99 [22], an industry standard for modeling atmospheric properties and dispersions. It provides complete geographic and temporal variations (though temporal variations are not studied in this work), rather than a standard atmosphere that only provides variations with respect to altitude. It also simulates position-dependent and altitude-dependent perturbations in the mean atmosphere. The strength of these factors is controlled through a parameter known as RPSCALE. This is a scale factor on the 1-σ variation about the nominal atmospheric parameters. The nominal value of RPSCALE is 1.0, which is used throughout all simulations. One hundred dispersed profiles of the GRAM07 atmosphere are shown in Fig. 6 relative to the 1976 U.S. Standard Atmosphere. Note the large magnitudes of dispersions in the upper atmosphere, but the smaller dispersions near the ground.

It should be noted that navigation uncertainties are not considered here. However, it is well recognized that the uncertainties of state-of-the-art navigation systems are not primary factors affecting the performance of the entry guidance system.

C. Simulation Results

Several different entry mission scenarios are tested. They correspond to different downrange distances and approach directions, resulting from different lunar-return conditions. The initial conditions are given in Table 2. The first mission in Table 2 has a short initial downrange of only 2200 km. There will be no skip trajectory for this mission. It is selected to test how the algorithm automatically adapts to such cases. All the missions are run under exactly the same settings, without any mission-dependent adjustments of guidance parameters or logic.

For each mission, 10,000 dispersion runs are performed. The guidance cycle is set at 1 Hz. The Orion CEV program has a landing precision requirement of 5 km [19]. Therefore, in testing, when the final position of the vehicle in a dispersed 3-DOF simulation is within 2.5 km of the landing site, it is considered a successful run, because the remaining 2.5 km is allocated for parachute drift. Any trajectory ending outside the 2.5-km radius but within the 5-km radius is regarded as a 50% success. Any trajectory ending outside the 5-km radius from the landing site is regarded as a failure.

In Fig. 7, a plot of the nominal altitude versus downrange clearly shows the skip out of the atmosphere for the northbound medium-range case (8400 km). The complete bank-angle history is shown in Fig. 8 and only the skip phase is shown in Fig. 9. The spike in bank angle appearing around 175 s in Fig. 8 is the spacecraft rolling from −100 through 180 deg to a positive bank angle, which can be seen more clearly in Fig. 9. By rolling through full lift down, the net effect is to maintain the maximum margin in bank-angle capability. The resultant command by the time the bank reaches the opposite side is slightly smaller than it was at the beginning, owing to the energy dissipated during the reversal. The ground track for the northbound skip entry trajectory is given in Fig. 10. The ground track for the eastbound skip entry also appears in Fig. 10. The altitude profile for a nominal eastbound medium-range (7300-km) skip entry is very similar to Fig. 7. The bank-angle time history is very similar to Fig. 8.

In Fig. 11, the altitude versus downrange is shown for 100 dispersed trajectories for the northbound medium-range skip entry. All the trajectories follow a similar path in the downward part of the skip phase; however, they differ considerably during the upward part of the skip phase and Kepler phases. With the normal start of the final

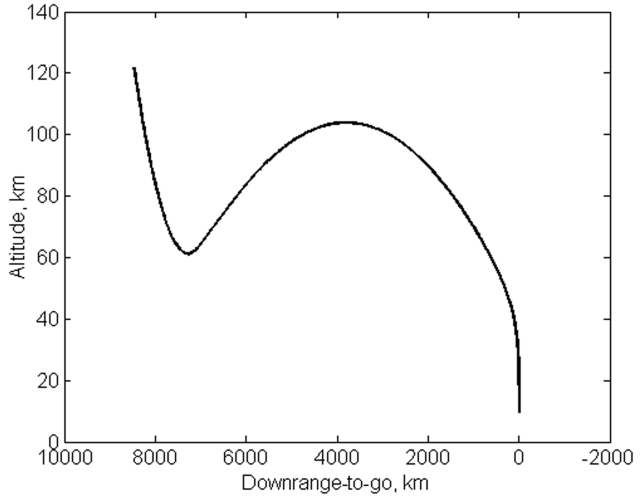

Fig. 7 Altitude versus downrange-to-go for the nominal northbound medium-range case (8400 km).

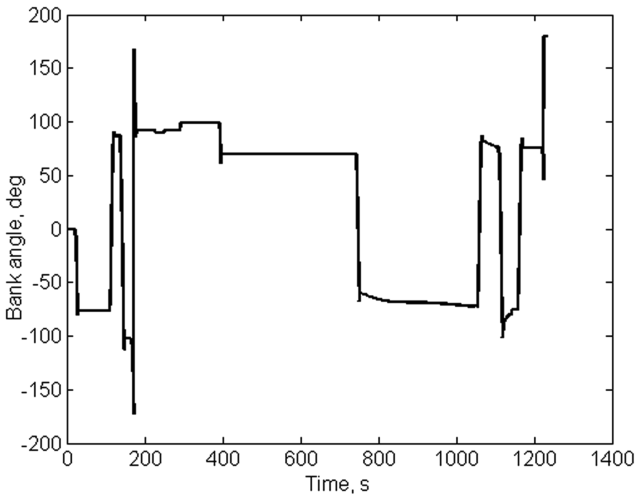

Fig. 8 Bank-angle profile for the nominal northbound medium-range case (8400 km).

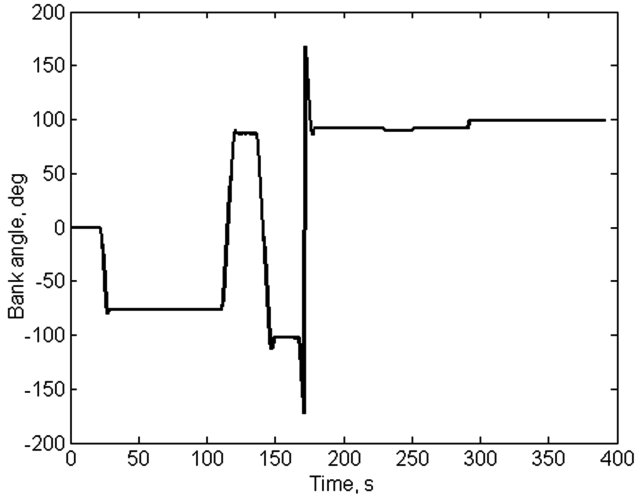

Fig. 9 Close-up view of the bank-angle profile during skip phase for the nominal northbound medium-range case (8400 km).

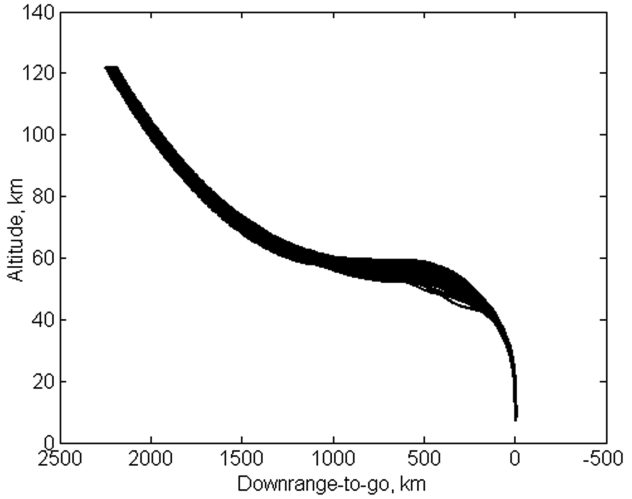

Fig. 12 Altitude versus downrange-to-go for 100 dispersed trajectories (northbound, 2200 km).

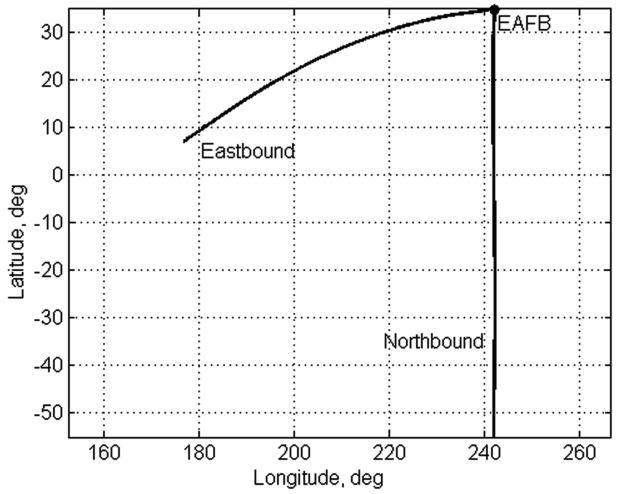

Fig. 10 Ground tracks for the nominal northbound and eastbound cases.

phase with 2000 km downrange-to-go, the final-phase guidance has to respond to up to 13-km differences in altitude at this point. These kinds of dispersions would likely severely stress the Apollo final-phase guidance. But with the seamless integration of the current skip guidance and final-phase-guidance algorithm in [17], precision landing is still achieved reliably.

Similarly, the altitude histories of 100 dispersed trajectories for the short-range (2200-km) eastbound mission are plotted in Fig. 12. Although the nominal trajectory for this mission is a direct-entry trajectory, some of the dispersed trajectories are actually loft trajectories, as can be seen in Fig. 12. The guidance algorithm automatically adapts to both direct-entry and loft-entry cases without difficulty. The load histories for 100 dispersed northbound trajectories are shown in Fig. 13. The average peak load is about 4.2 *g* during the skip phase and about 5 *g* in the final phase. No load-relief maneuvers are taken. However, if necessary, a predictive load-relief strategy developed in [17] can be applied in the final phase.

In Figs. 14 and 15, the final locations of the 10,000 dispersed entry trajectories for two missions are shown. The other northbound missions have plots very similar to Fig. 14. In all cases except for one in the northbound long-range (10,000-km) mission, the vehicle's position is within 2.5 km of the landing site at the termination of entry guidance. The failure case will be discussed further, shortly. Table 3 summarizes the final position statistics for 10,000 dispersed trajectories for each of the missions in Table 2.

The long-range (10,000-km) mission has one case that fails to terminate within 5 km of the landing site. In this case, the trajectory

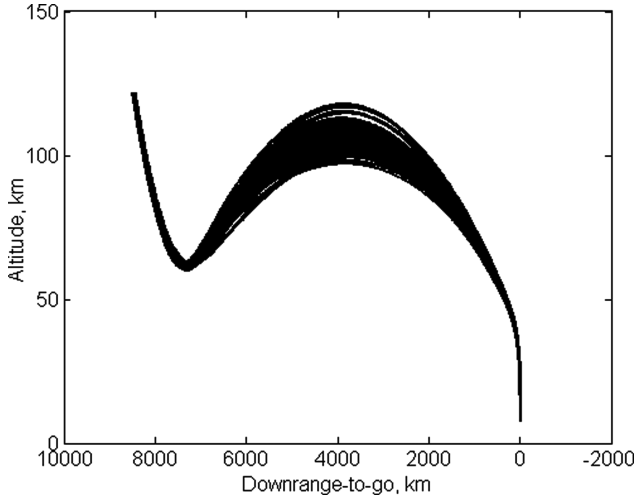

Fig. 11 Altitude versus downrange-to-go for 100 dispersed trajectories (northbound, 8400 km).

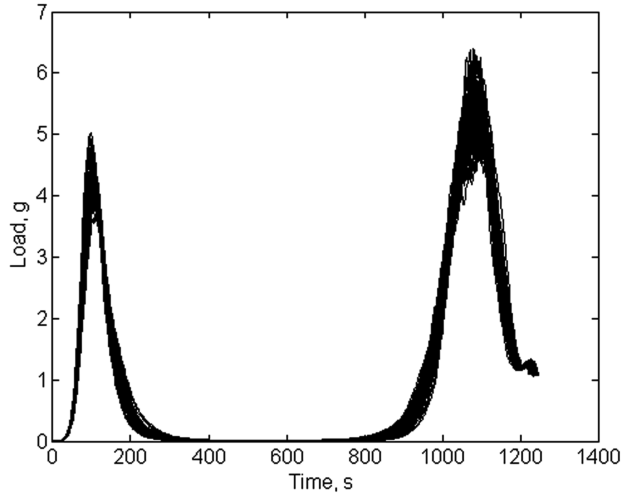

Fig. 13 Time history of load for 100 dispersed trajectories (northbound, 8400 km).

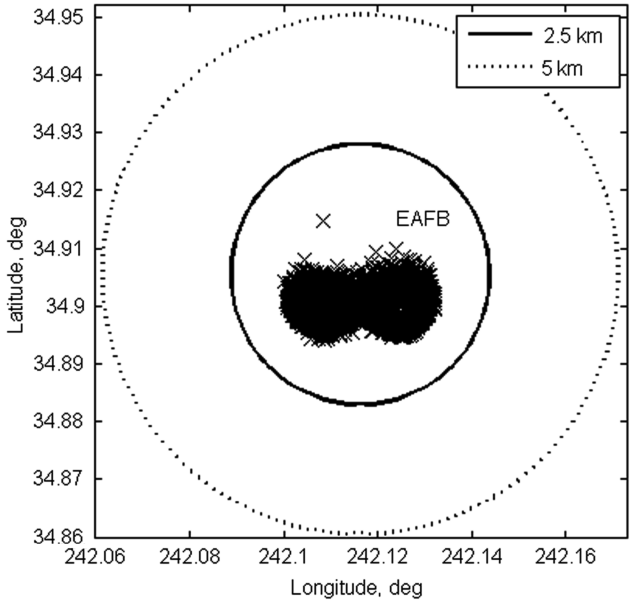

Fig. 14 Final positions of 10,000 dispersed trajectories for the northbound direct case (2200 km).

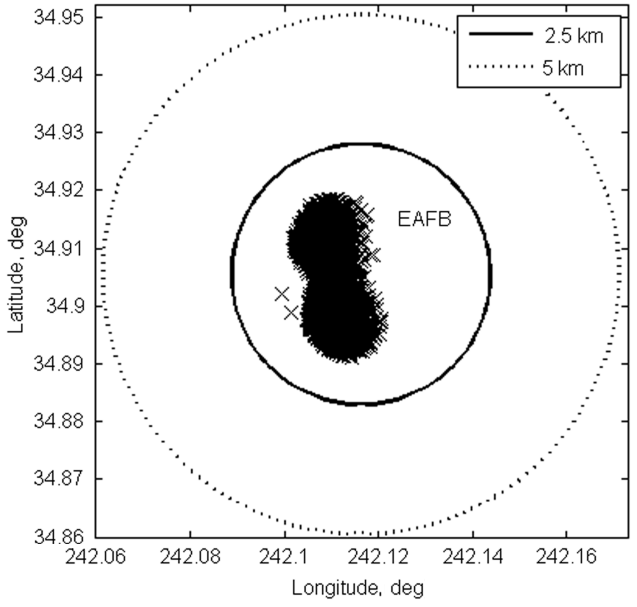

Fig. 15 Final positions of 10,000 dispersed trajectories for the eastbound medium-range case (7300 km).

misses the landing site by 15 km. A closer examination reveals that the reasons for the failure are the simultaneous concurrence of a particular pattern of the relatively extreme dispersion in atmospheric density and an appreciable dispersion (about 20% reduction) in L/D. In Fig. 16, the ratio of the GRAM07 dispersed density (ρ_{true}) to the U.S. 1976 standard atmosphere (ρ_{model}) is shown for the case. The dispersed atmosphere is over 40% thicker during the downward

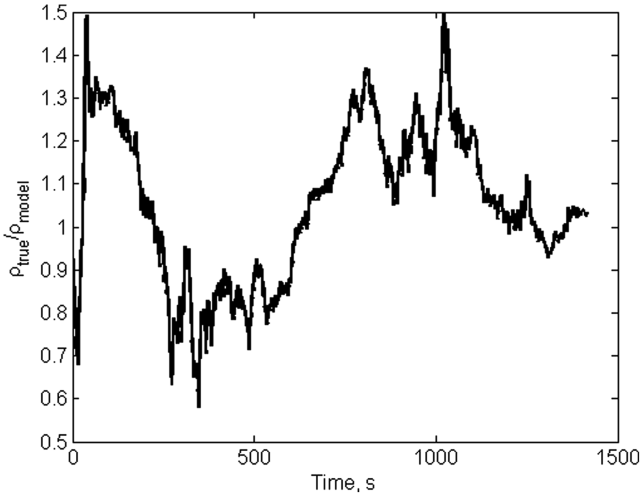

Fig. 16 Ratio of the GRAM07 atmosphere (ρ_{true}) to the U.S. 1976 Standard Atmosphere (ρ_{model}) for the failed northbound long-range case (10,000 km).

phase of the skip. The extreme thickness in atmospheric density relative to the modeled value early in the entry trajectory causes the vehicle to fly a relatively small bank angle, as seen in Fig. 17. Subsequently, the atmospheric density rapidly thins, which, together with the reduction in L/D, requires the vehicle having to fly a 180-deg bank angle to deplete enough energy during the remainder of the skip phase. However, this maneuver leaves no lateral control on the trajectory. Consequently, as the vehicle enters the final phase after the Kepler phase, the crossrange is larger than expected, despite the targeting bias. The rapid reduction in bank angle in Fig. 17 near the end of the trajectory is a reflection of the guidance detecting that there is still a distance to cover to the landing site as the velocity approaches the specified terminal value. This distance, however, is due to crossrange error. As the vehicle passes (laterally) by the landing site, the guidance commands full lift down to quickly terminate the entry trajectory, yielding a miss distance of 15 km.

If the atmospheric-density profile could be known in advance to have the shape as in Fig. 16, the guidance could use this information so that in the downward part of the skip phase, a sufficiently large bank angle would be commanded, and this case would have been saved. Because the actual atmospheric-density profile ahead would be impossible to predict closely, it seems unlikely that the predictor–corrector guidance (or any other guidance) could do more to alleviate such an extreme event. As it currently stands, the guidance achieves a 99.998% success rate in this more difficult mission. A risk assessment to examine the likelihood of an event of the preceding particular nature and magnitudes in long-range skip entry missions would help determine if further improvement is warranted.

VI. Conclusions

A method of skip entry guidance for a vehicle with a low L/D ratio is developed. The approach combines both onboard skip trajectory planning and closed-loop guidance in one. Unlike the Apollo skip entry guidance, the algorithm computes the bank angle required to achieve the final range condition and the corresponding trajectory based on numerical solution of the full 3-DOF dynamics, without

Table 3 Statistics on final miss distances in 10,000 dispersed trajectories

Miss distance, km	Northbound direct	Northbound short range	Northbound medium range	Northbound long range	Eastbound medium range
Average	0.939	0.984	0.968	0.930	0.882
Median	0.908	1.009	0.952	0.898	0.818
Maximum	1.597	1.618	1.792	2.335[a]	1.664
Minimum	0.071	0.137	0.042	0.073	0.075
Standard deviation	0.316	0.305	0.317	0.423	0.312

[a]See the further discussion in Sec. V.C concerning one failure omitted from this statistic.

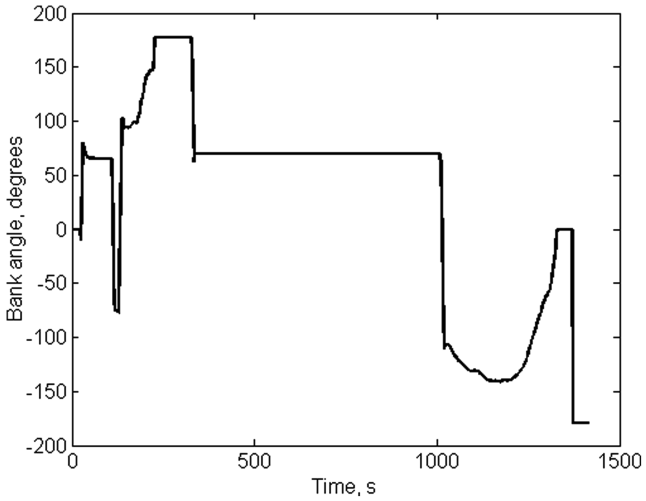

Fig. 17 Bank-angle history for one the failed northbound long-range case (10,000 km).

further assumptions or simplifications. No particular patterns of the trajectory are assumed. As a result, the algorithm is able to transition seamlessly between different phases of the skip trajectory and reliably adapts to different trajectory patterns, regardless of whether the entry trajectory actually skips out of the atmosphere. Several implementation issues are found to be critical to the performance and robustness of the algorithm. They include appropriate direction for bank-angle reversals, automated targeting bias for long skip trajectories, and proper use of lift and drag acceleration filters for enhanced robustness with respect to modeling uncertainties. The success of the algorithm in extensive, stressful, 3-DOF, end-to-end dispersion simulations clearly demonstrates the high performance and robustness of the algorithm for a wide range of mission scenarios.

References

[1] Moseley, P. E., "The Apollo Entry Guidance: A Review of the Mathematical Development and its Operational Characteristics," TRW, Inc., Rept. 69-FMT-791, Houston, TX, Dec. 1969.

[2] Graves, C. A., and Harpold, J. C., "Apollo Experience Report—Mission Planning for Apollo Entry," NASA TN D-6725, Mar. 1972.

[3] Kuo, Z., and Vinh, N. X., "Improved Matched Asymptotic Solutions for Three-Dimensional Atmospheric Skip Trajectories," *Journal of Spacecraft and Rockets*, Vol. 34, No. 4, 1997, pp. 496–502.

[4] Istratie, V., "Optimal Skip Entry into Atmosphere with Minimum Heat and Constraints," AIAA Paper 2000-3993, Aug. 2000.

[5] Bairstow, S. H., "Reentry Guidance with Extended Range Capability for Low L/D Spacecraft," M.S. Thesis, Dept. of Aeronautics and Astronautics, Massachusetts Inst. of Technology, Cambridge, MA, Feb. 2006.

[6] Putnam, Z. R., Braun, R. D., Bairstow, S. H., and Barton, G. H., "Improving Lunar Return Entry Range Capability Using Enhanced Skip Trajectory Guidance," *Journal of Spacecraft and Rockets*, Vol. 45, No. 2, 2008, pp. 309–315.

[7] Tigges, M. A., Crull, T., and Rea, J. R., "Numerical Skip Entry Guidance," American Astronautical Society Paper 07-076, Feb. 2007.

[8] Carman, G. L., Ives, D. G., and Geller, D. K., "Apollo-Derived Mars Precision Lander Guidance," AIAA Paper 98-4570, Aug. 1998.

[9] Bryant, L. E., Tigges, M. A., and Ives, D. G., "Analytic Drag Control for Precision Landing and Aerocapture," AIAA Paper 98-4572, Aug. 1998.

[10] Lu, W.-M., and Bayard, D. S., "Guidance and Control for Mars Atmospheric Entry: Adaptivity and Robustness," Jet Propulson Lab., California Inst. of Technology, Pasadena, CA, Jan. 1999.

[11] Tu, K.-Y., Munir, M. S., Mease, K. D., and Bayard, D. S., "Drag-Based Predictive Tracking Guidance for Mars Precision Landing," *Journal of Guidance, Control, and Dynamics*, Vol. 23, No. 4, 2000, pp. 620–628.

[12] Hanson, J. M., "Combining Propulsive and Aerodynamic Maneuvers to Achieve Optimal Orbital Transfer," *Journal of Guidance, Control, and Dynamics*, Vol. 12, No. 5, 1989, pp. 732–738.

[13] Schottle, U. M., Burkhardt, J., and Zimmermann, F., "Optimal Flight Control of a Reentry Capsule with Consideration of Mission Constraints," AIAA Paper 97-3659, 1997.

[14] Gamble, J. D., Cerimele, C. J., Moore, T. E., and Higgins, J., "Atmospheric Guidance Concepts for an Aeroassisted Flight Experiment," *Journal of the Astronautical Sciences*, Vol. 36, No. 1, 1988, pp. 45–71.

[15] Powell, R. W., and Braun, R. D., "Six-Degree-of-Freedom Guidance and Control Analysis of Mars Aerocapture," *Journal of Guidance, Control, and Dynamics*, Vol. 16, No. 6, 1993, pp. 1038–1044.

[16] Evans, S. W., and Dukeman, G. A., "Examination of a Practical Aerobraking Guidance Algorithm," *Journal of Guidance, Control, and Dynamics*, Vol. 18, No. 3, 1995, pp. 471–477.

[17] Lu, P., "Predictor-Corrector Entry Guidance for Low Lifting Vehicles," *Journal of Guidance, Control, and Dynamics* (accepted for publication).

[18] Vinh, N. X., *Optimal Trajectories in Atmospheric Flight*, Elsevier Scientific, New York, 1981, pp. 58, 60.

[19] Rea, J. R., and Putnam, Z. R., "A Comparison of Two Orion Skip Entry Guidance Algorithms," AIAA Paper 2007-6424, Aug. 2007.

[20] Zarchan, P., and Musoff, H., *Fundamentals of Kalman Filtering: A Practical Approach*, 2nd ed., Progress in Astronautics and Aeronautics, Vol. 208, AIAA, Reston, VA, 2005, p. 647.

[21] D'Souza, C., Crain, T., Clark, F. D., and Getchius, J., "Orion Cislunar Guidance and Navigation," AIAA Paper 2007-6681, Aug. 2007.

[22] Justus, C. G., and Johnson, J. L., "The NASA/MSFC Global Reference Atmospheric Model—1999 Version (GRAM-99)," NASA TM-1999-209630, 1999.